Movie

SPH simulations of magnetic fields in galaxy clusters

Klaus Dolag[1], Matthias Bartelmann[1] & Harald Lesch[2]

[1] Max-Planck-Institut für Astrophysik, P.O. Box 1523, D-85740 Garching, Germany

[2] Universitäts-Sternwarte München, Scheinerstr. 1, D-81679 München, Germany

0 Introduction and Summary

Observations consistently show that clusters of galaxies are pervaded by magnetic fields of $\sim\mu$G strength. Coherence of the observed Faraday rotation measures on source scales demonstrates that the fields at least have a field component that is smooth on cluster scales. The origin of such fields is largely unclear. Models invoking primordial magnetic fields are required to produce magnetic fields in the course of cluster formation to the observed present-day strengths, which are orders of magnitude too low for adiabatic compression alone. We investigate what kind of initial magnetic fields are required to produce magnetic fields in the course of cluster formation that are able to reproduce observations like Faraday rotation and cluster radio halos.

We start cosmological simulations of clusters with an initial magnetic field of $|\vec{B}|(z=20)=10^{-9}$G at a regime of $z=15$, which reaches the observed $\sim\mu$G field strengths in the cluster cores at $z=0$.

The main results of our simulations are:

- While simple collapse models predict final field strengths of $\sim 0.1\,\mu$G only, additional field amplification by shear flows in clusters produces the observed $\sim\mu$G fields.
- The final field configuration in the clusters is dominated by the cluster collapse, so that the initial field configuration, which is assumed to be homogeneous initial fields lead to Faraday rotation measures that can not significantly be distinguished.
- Synthetic RM observations obtained from our simulations agree very well with real observations in the best-observed clusters, Coma and A 2199, when starting with 10^{-9}G fields.
- Filling our simulated clusters with a relativistic power-law electron component, we are able to reproduce radio halos without over-producing hard Universe-Comptonized X-Ray emission.

1 Faraday Rotation

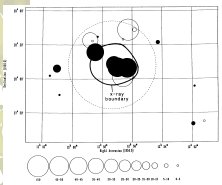

Figure 1. Rotation measures observed in the Coma cluster (Kim et al. 1991). The size of the circles indicates the absolute value of RM, the type filled or empty) the sign of RM. The X-ray boundary (solid curve) and the Abell radius (dashed circle) are superposed to mark the position of the Coma cluster in the plot. The RM pattern can later be compared with our simulated results.

2 GrapeMSPH

Our code simultaneously computes with a multiple time-step scheme the behavior of two matter components, a dissipation-free dark matter component interacting only through gravity, and a dissipational, gaseous component. We supplemented the code with the magneto-hydrodynamic equations to follow the evolution of an initial magnetic field caused by the flow of the gaseous matter component.

- The gravitational interaction is calculated on the special-purpose hardware component Grape 3Af, in which the Plummer law is hard-wired.
- The hydrodynamics is calculated in the smooth-particle approach (SPH; Lucy, Monaghan). This method replaces test particles by spheres with variable radii, which are adapted to the local density. This results in an adaptive resolution.
- The treatment of the magnetic field assumes the ICM is a plasma with large conductivity. In this case the Maxwell equations are simplified to the usual induction equation.

In principle, it is not guaranteed that $\nabla\cdot\vec{B}$ vanishes, but our show that it stays negligible throughout all of our cluster runs. In general, the magnetic field remains dynamically unimportant in our simulated clusters. We extensively tested the code with test problems to ensure it works reliably for our purposes.

3 The final set of equations

The momentum equation then can be written

$$\begin{aligned}\frac{\mathrm{d}\vec{v}_i}{\mathrm{d}t} = &-\sum_j m_j\left(\frac{P_i}{\rho_i^2}+\frac{P_j}{\rho_j^2}+\Pi_{ij}\right)\nabla_i W(\vec{r}_i-\vec{r}_j,h)\\ &+\sum_j m_j\left[\left(\frac{\mathcal{M}_i}{\rho^2}\right)_i+\left(\frac{\mathcal{M}_{ij}}{\rho^2}\right)_j\right]\nabla_{r_i}W(\vec{r}_i-\vec{r}_j,h)\\ &-\sum_j\frac{m_j}{(|\vec{r}_i-\vec{r}_j|+0.25(v_i+v_j)^{2/3}}(\vec{r}_i-\vec{r}_j) \qquad (1)\\ &+\Omega_i\vec{H}_i^2\vec{x}_i\end{aligned}$$

and the energy equation takes the form

$$\frac{\mathrm{d}u_i}{\mathrm{d}t}=\frac{1}{2}\sum_j m_j\left(\frac{P_i}{\rho_i^2}+\frac{P_j}{\rho_j^2}+\Pi_{ij}\right)(\vec{v}_i-\vec{v}_j)\nabla_i W(\vec{r}_i-\vec{r}_j,h)\,.$$

These equations need to be supplemented by an equation of state. We assume an ideal gas with an adiabatic index of $\gamma=5/3$, for which the pressure is given by $P_i=(\gamma-1)u_i\rho_i$. The tensor Π_{ij} describes an artificial viscosity term required to properly capture shocks (Monaghan & Gingold 1983). The magnetic stress tensor $\mathcal{M}_{ij}$ is defined as

$$\mathcal{M}_{ij}=\frac{1}{4\pi}\left(B_iB_j-\frac{1}{2}B^2\delta_{ij}\right)$$

(Phillips & Monaghan 1985). In the language of SPH, the induction equation reads

$$\frac{\mathrm{d}\vec{B}_{i,j}}{\mathrm{d}t}=\frac{1}{\rho_i}\sum_k m_k(\vec{B}_{i,k}\vec{v}_{ik}-\vec{v}_{ik}\vec{B}_i)\nabla_i W(\vec{r}_i-\vec{r}_k,h).$$

The code uses a multiple time-step scheme to speed up calculation and is based on the GrapeSPH code developed and kindly provided my Matthias Steinmetz (Steinmetz 1996).

4 Initial conditions

We need two types of initial conditions for our simulations:

- The cosmological parameters.
  So far, we set up cosmological initial conditions in an Einstein-de Sitter universe ($\Omega_\Lambda=1,\Omega_\circ=0$) with a Hubble constant of $H_\circ=50\,\mathrm{km\,s^{-1}\,Mpc^{-1}}$. We initialize density fluctuations according to a COBE-normalized CDM power spectrum.
- The properties of the primordial magnetic field.
  The simulations presented here start with two extreme set-ups of the primordial magnetic field, namely either a chaotic or a completely homogeneous magnetic field at high redshift. The average magnetic field strength is fixed to the same value in both cases to allow a fair comparison of the results. We also vary the strength of the initial magnetic field.

Our simulations work with three classes of particles. In a central region, we have $\approx 50,000$ collision-less dark-matter particles with mass $\approx 3.2\times 10^{13}\,M_\odot$, mixed with an equal number of gas particles whose mass is twenty times smaller. This is the region where the cluster is form. The central region is surrounded by $\approx 20,000$ collision-less boundary particles whose mass increases outward to mimic the tidal forces of the neighboring large scale structure.
For computational reasons, we superpose the magnetic field to the initial data at $z=15$, but the exact initial redshift does not matter as long as the magnetic field is put into the simulations, before the onset of cluster formation. For example, an initial magnetic field of $|\vec{B}|^{(z)}=10^{-9}$ G at a redshift of $z=15$, decrease to $\approx 0.2\times 10^{-9}$ G at $z=4$ due to cosmic expansion, without any noticable impact of cluster collapse.

5 The simulated clusters

The amplification of the magnetic field in a volume element during the cluster formation depends on the direction of the magnetic field relative to the motion of the volume element. It is therefore not expected that the magnetic field in a cluster acquires an orderly radial profile like, e.g., the density. A randomly magnetized sphere, spherically collapsing due to gravity leads to an enhancement of the magnetic field proportional to $\rho^{2/3}$. For galaxy cluster, starting with magnetic field strengths of order 10^{-9} G, this can only produce fields of 10^{-7} G strength. In our simulations, however, this seed fields are indeed amplified to reach 10^{-6} G in final stages of cluster evolution. This is due to shear flows which tangle the magnetic field and thus help amplify it.

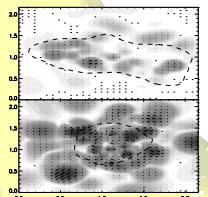

Figure 2. This figure shows slices and projections of a simulated cluster. The grey-scale encodes absolute magnetic field strength as indicated below the panels. The arrows mark magnetic field vectors in the planes of the slices. Notice that lengths, field strengths, and magnetic field vectors are scaled in the same way in both panels. The contour encloses the region emitting 95% of the slices' total X-ray luminosity. The cluster shown in the upper panel is highly substructured, which can be seen from the elongated X-ray contour. Therefore, the X-ray region is more extended than in the more compact and twice massive cluster shown in the lower panel. This more massive cluster has a stronger magnetic field, due to the larger amount of compression of gas during its formation.

6 X-Ray emission and Radio Halo

The resolution of our simulations is not good enough to accurately describe in detail the radio halo of a simulated cluster. Describing the mean magnetic field in clusters and ignoring small-scale fluctuations, our simulations can only provide a lower limit to the radio emission. So far, we have only briefly investigated one question:

- Using a power-law electron distribution, with a slope adapted to the observations and its normalization chosen to produce the radio luminosity, did the relativistic electron population show up in the X-Ray emission ?
  The relativistic electrons give rise to hard X-ray emission due to inverse Compton scattering of the cosmic microwave background photons. Using the population of relativistic electrons as mentioned before we calculated the inverse-Compton emission to find it negligible compared to thermal emission in the soft X-ray bands, which is in general agreement with observations.

We will investigate this in more detail as soon as higher resolution simulations will be available. Nevertheless, the previous comparison closes the consistent picture of the clusters in our simulations.

Movie

7 The simulated RM maps

Observing a background radio source through a galaxy cluster at different wavelengths and measuring the position angle ϕ of the polarization allows to determine the rotation measure,

$$\mathrm{RM}=\Delta\phi\frac{\lambda_2\lambda_1}{\lambda_2-\lambda_1}=\frac{e^3}{2\pi m_e^2c^4}\int n_e\vec{B}\,\mathrm{d}\vec{l}\,.$$

It can have either sign, depending on the orientation of the magnetic field.

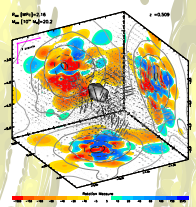

Figure 3. This figure shows one of the most massive simulated clusters in a three-dimensional box. The Faraday rotation measures produced by the cluster in the three independent spatial directions are projected onto the box sides and encoded by the color-scale as indicated below the box. The grey solid curves are projected density contours. They are scaled as $\frac{1}{3},\frac{1}{2},\frac{2}{3},\frac{3}{4},\frac{4}{5}$ and $\frac{5}{6}$ of the mean over the maximums of the three projection directions. The $\frac{1}{2}$ level is marked by the dashed line. The white dashed curve encompasses the region emitting 90% of the projected X-ray luminosity. The shaded circle in the center is the 1D-Surface of halve the central density. Additional the 1D magnetic field vectors are plotted. To improve the 1D effect, they are grey-scaled to indicate the radial distance from the center. Therefore they are plotted black in the center and get brighter towards the edges of this plot. The cluster is taken from output data at redshift $z=0.4$. The plotted coordinates are physical coordinates, the virial mass is and the virial radius are indicated in the plot.

8 A comparison with Coma

We can now compare the simulated clusters for different initial conditions or compare them with measurements in individual clusters like Coma, for which some measurements are available. We therefore shoot beams through the simulated clusters and compare the synthetic rotation measure samples statistically.

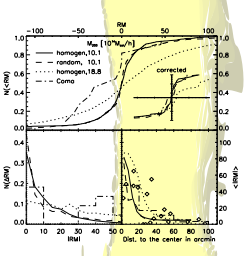

Figure 4. This figure shows different visualizations of the RM statistics for a simulated cluster with two different types of initial conditions for the magnetic field, namely homogeneous (solid line) and chaotic (dashed line). A more massive cluster (dotted line) and the RM values observed in the Coma cluster (dash-dotted line respectively) are overlayed for comparison. It is evident in all panels that the RM samples are statistically indistinguishable for the two different types of initial conditions. Due to the stronger magnetic field and therefore the larger area with high RM values, the more (approx. two times massive) cluster give significant better statistics. The top panel shows cumulative distributions of rotation measures. Obtaining randomly 81 values in a way to match the distance distribution for the Coma measurements, the Kolmogorov-Smirnov test gives a thirty percent chance for the observation to be drawn from the simulated distributions for the smaller cluster. Hence, the observations in Coma cannot significantly be distinguished from the simulated rotation measures. Conversely, this means that the simulations well reproduce the rotation-measure pattern observed in Coma. For the more massive cluster, the probability for the Coma data to be drawn from the simulated distributions goes to one percent. The additional plot in the upper panel shows the final comparison with the Coma measurement, applying some corrections for intrinsic RM value and spatial distribution of the sources. The lower left panel shows the distribution of the RM measurements inside the X-Ray boundary. The more massive cluster has relatively more high and lower low RM values than the less massive one. The lower right panel shows the mean of the absolute value for the RM measurements as function of the distance to the cluster center. Towards its center, the more massive cluster has to high RM values compared to Coma, while the less massive one almost reproduces the observation. In the outer parts, both cluster predict too small RMs.

9 A comparison with a cluster sample

Unfortunately, in most clusters the number of radio sources suitable for measurements of Faraday rotation is only one or two. We therefore also compare a sample of simulated clusters with a compilation of RM observations in different clusters. We use the observational data published by Kim et al 1991.

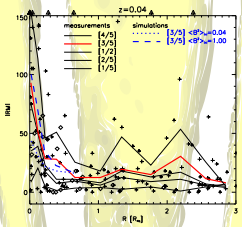

Figure 5. The absolute values of Faraday rotation measurements (Kim et al. 1991) vs. radius in units of the Abell radius are shown. Obviously, the dispersion decreases towards the cluster center. In outer parts it is dominated by a few sources, which in some cases even fall outside the plotted region and are marked by the arrows at the top of the plot, we did not calculate the variance, but rather the percentiles of the RM distribution. Thin lines mark the RM value, which contains 20%, 40%, 60%, 80% and 95% of the measurements in each radial bin. The radial bins are chosen such as to contain 6 data points each. Changing the number to 12 did not alter the results at all. The heavy, non-solid lines finally are synthetic rotation measures obtained from our simulations, for which we have chosen the 68% level. The different lines are corresponding to different values of the initial magnetic field energy, as indicated in the plot. They can be compared with the measurements which are marked with the heavy solid line (cf. for the 68% level). The output was taken at $z=0.04$.